A Crystal Modulating Protein from Molluscan Nacre That Limits the Growth of Calcite in Vitro

Il Won Kim,[†] Sebastiano Collino,[†] Daniel E. Morse,[‡] and John Spencer Evans*,[†]

Laboratory for Chemical Physics, New York University, 345 East 24th Street, New York, New York 10010, and Center for Collaborative Biotechnologies, Department of Molecular, Cellular, and Developmental Biology, University of California, Santa Barbara, Santa Barbara, California 93106

ABSTRACT: Protein-mediated biomineral formation and polymorph selection in the mollusk shell involves the participation of a number of different proteins. One of these proteins, AP7, has been identified as a participant in nacre (aragonite) formation in the mollusk *Haliotis rufescens.* However, the role(s) of this protein in aragonite formation is (are) poorly understood, due to the fact that low quantities of this protein are recoverable from the nacre matrix. To overcome this problem, we employed stepwise solid-phase tBOC synthesis to recreate the 66-AA single-chain protein AP7 and utilized this synthetic form for in vitro mineralization studies. We find that the AP7 protein promotes incomplete or interrupted crystal growth and step edge roundening in a concentration-dependent fashion. Using synthetic peptides which represent the 30-AA N-terminal (AP7N) and 36-AA C-terminal (AP7C) subdomains of AP7, we have identified that the mineral modification activity of AP7 is localized to the unstructured, conformationally labile N-terminal subdomain. Interestingly, the 36-AA C-terminal subdomain has no observable direct effect on in vitro calcium carbonate crystal growth; however, we cannot rule out the possibility that AP7C plays an indirect role in AP7 mineralization activity. Qualitative structural studies reveal that AP7, although possessing Zn(II) fingerlike −His−(X)$_6$−His, −Cys-(X)$_2$−Cys−, and −Cys−(X)$_4$−Cys− motifs within its C-terminal region, does not possess the structural characteristics of known Zn(II) finger polypeptides, as evidenced by the presence of an ordered, α-helical conformation within the C-terminal subdomain of apo-AP7. Given its associative nature with AP24 and the multifunctional capabilities of the 30-AA N-terminal domain, it is likely that the AP7 protein possesses multifunctional capabilities with regard to nacre formation within the mollusk shell.

One of the more interesting phenomena in biomineralization is the process of inorganic polymorph formation: i.e., the nucleation and growth of inorganic solids which possess the same ionic components but differ in their structural arrangement. For example, in some mollusk shells, two different polymorphs of calcium carbonate (CaCO$_3$), calcite and aragonite, coexist as the adjacent prismatic and nacreous layers of the shell, respectively.[1−6] Biologists have long been intrigued by the fact that two different calcium carbonate polymorphs develop simultaneously within the shell under ambient conditions. The formation of each polymorph is believed to be under the control of a number of unique protein superfamilies which are specific for a given shell layer.[1−10] Not surprisingly, recent sequencing studies reveal that nacre-[3,6−8] and prismatic-associated[9] proteins possess a number of fundamental differences at the level of primary sequence and amino acid composition. At this time it is not known how these various proteins control and modulate polymorph selection within the mollusk shell, nor is it known what important sequence features are required for this process in situ. However, it is clear that attaining the molecular mechanism(s) involved in these protein-mediated processes would be of tremendous benefit to both biology and to the materials science /nanotechnology communities.

Recently, progress has been made in identifying key protein participants in the polymorph selection process within the nacre[5,7,8] and prismatic[9−11] layers of invertebrate shells. As an example, a series of proteins associated with aragonite formation in the nacre layer of the Pacific Red abalone, *Haliotis rufescens,* have been identified and sequenced.[5,11] In vitro mineralization studies have indicated that two of these proteins, AP7 and AP24, coexist as a complex that jointly limits the growth of calcite.[5] Subsequent studies involving AP7- and AP24-derived model peptides revealed that both proteins possess mineral modification domains at their N-termini.[5,12] However, further studies of AP7 and AP24 have been hampered by a number of factors: the limited availability of these proteins from nacre matrix, the strong associative interactions between both proteins which complicates isolation, and the inability to overexpress

these proteins via recombinant techniques at the present time. As a result, very little is known regarding the individual contributions of each protein to the overall process of limiting calcite growth within in vitro settings.

To circumvent these problems, we have explored the application of chemical synthesis techniques (highly optimized stepwise solid-phase peptide synthesis)[11−18] to create nacre-specific proteins that are relatively small (i.e., 50−80 AA) and free of posttranslational modifications which would complicate the de novo reconstruction of the protein. Here, we report the first successful synthesis, purification, and preliminary characterization of the smaller nacre protein AP7 (66 AA, 7.5 kDa, Figure 1).[5] This protein is isolated from nacre mineral in the free disulfide form under nonreducing conditions and does not contain intra or inter −S−S− linkages.[5] Using tBoc-based direct sequential synthesis techniques,[13−20] we have created a synthetic version of AP7 in the free thiol form. Using comparative in vitro assays, we demonstrate that the synthetic AP7 protein frustrates or inhibits calcite crystal growth in a manner consistent with the previously reported activity of the N-terminal 30 AA subdomain AP7N,[21] in general agreement with previous findings obtained for nacre-purified AP7−AP24 complex.[5] To assist in our interpretations, a synthetic peptide representing the 36-AA AP7C segment (Figure 1) was also created, and we find that AP7C exhibits no observable effect on in vitro calcium carbonate crystal growth, indicating that the C-terminal 36-AA segment does not directly affect mineralization by itself. From a structural standpoint, the solution secondary structure of synthetic AP7 consists of unstructured and α-helical regions, and comparative studies performed with both AP7N and AP7C confirm that it is the 30-AA N-terminal subdomain of AP7 which is unstructured, whereas the 36-AA C-terminal region is α-helical.

Materials and Methods. (a) Solid-Phase Synthesis and Purification. We employed a tBoc-based stepwise solid-phase synthesis[13−20] to create AP7, since tBoc chemistries have the advantage of clean, reliable, and rapid acidolytic N^α-Boc deprotection compared with its Fmoc counterpart, which is prone to kinetically slower, sequence-dependent, and/or incomplete N^α-Fmoc deprotection.[13−20] The synthesis of free α-carboxyl AP7 in the free Cys-SH form was conducted at the Wm. Keck Biotechnology Peptide Synthesis Facility, Yale University, using Asn-trityl-PAM

* To whom correspondence should be addressed. E-mail: jse1@nyu.edu.
† New York University.
‡ University of California.

```
 1                10              20              30
DDNGNYGNGMASVRTQGNTYDDLASLISYL
31          40            50            60
TRHSFRRPFHECALCYSITDPGERQRCIDM
61      66
YCSYTN
```

AP7N = Gray

AP7C = Black

Figure 1. Primary amino acid sequence of *H. rufescens* nacre associated AP7 protein. The sequence represents mature, processed protein. Residues 1−30 represent the AP7N mineral binding domain (gray); residues 31−66 represent the AP7C domain (black).

(phenylacetamidomethyl) resin, a customized Applied Biosystems 432A peptide synthesizer, and standard *tert*-butoxycarbonyl (tBOC) chemistry with in situ neutralization.[13−20] N^α-tBOC protected amino acids were utilized for coupling, and specific side chain protection was used for the following amino acids: Cys (*S*-acetamidomethyl), Asn (*β*-trityl), Asp (*tert*-butyl ester), Arg (N^G-(4-tosyl)), Glu (*tert*-butyl), Gln (*β*-trityl), His (dinitrophenyl), Ser (*O*-benzyl), Thr (*O*-benzyl), Tyr (*O*-2-bromobenzyloxycarbonyl), Lys (N^ϵ-2-chlorobenzyloxycarbonyl). Double-volume, double-coupling procedures were primarily utilized, with coupling times ranging from 20 to 35 min, with the longer coupling times employed for side-chain-protected residues, particularly Cys. Resin cleavage and side-chain deprotection were conducted as described.[13] Cleaved AP7 was then solubilized with mixtures of water and trifluoroacetic acid (TFA; Sigma-Aldrich) and purified by preparative reverse-phase high-performance liquid chromatography (RP-HPLC) using a Waters DeltaPak C18 RP-HPLC column, with 0.1% TFA/water mobile phase and elution with 80% acetonitrile/0.1% TFA/water linear gradient (0−80% acetonitrile, 80 min). All running and elution buffers were purged with N_2 gas and degassed to remove any dissolved O_2 which might oxidize the free Cys thiol groups. The column elution was monitored at 230 nm, and individual HPLC fractions were analyzed using MALDI-TOF mass spectrometry. The purity of AP7 was determined to be 94%, based upon RP-HPLC rechromatography and MALDI-TOF of the purified protein (Figure 2). On the basis of a 100 *μ*mol synthesis, the total yield of purified AP7 was 13.5 mg. The experimental mass of singly charged AP7 was observed to be 7572.91 Da, within 6−7 Da of the observed mass for the nacre-purified, free thiol AP7, 7566 Da (Figure 2). The slightly higher molecular weight of synthetic AP7 confirms that no −S−S− bonds were formed postsynthesis. The double-charged species was also observed at 3787.42 Da (Figure 2). Purified AP7 was lyophilized and stored in a sealed tube under N_2 at −20° C until needed.

(b) CD Spectrometry. For subsequent experiments involving AP7 and AP7C, we employed published protocols utilized for Zn-(II) finger polypeptides to ensure reducing conditions and maintain free Cys −SH groups.[22−25] All deionized distilled water and buffer

The AP7N (free N-terminus, C-amide-capped-terminus) and AP7C (*N*-acetyl modified, free C-terminus) subdomain model peptides were both synthesized at the 100 *μ*mol level and purified at the Wm. Keck Biotechnology Peptide Synthesis Facility, Yale University, by Dr. Janet Crawford and staff, using previously published FMOC and RPLC protocols.[5,21] The AP7C polypeptide was synthesized, cleaved, and purified in the free Cys-SH form using the same precautions for Cys-SH oxidation during purification and storage as described for AP7. The experimental molecular masses for AP7N and AP7C were determined by matrix-assisted laser desorption ionization/time-of-flight mass spectroscopy (MALDI/TOF-MS; Yale University) to be 3226.7 and 4400.8 Da, respectively, in agreement with the theoretical molecular masses of 3226.4 and 4400.9 Da, and indicate that AP7C was successfully synthesized in the free thiol form.

Figure 2. (A) Reverse-phase HPLC chromatography of purified AP7 protein. (B) MALDI-TOF mass spectra of purified AP7 protein, with the detector optimized for singly and doubly charged species.

solutions were bubbled/purged with N_2 for at least 15 min in all subsequent experiments to minimize possible Cys thiol oxidation from dissolved O_2 and then kept sealed until used.[22−25] Likewise, sample solutions were kept sealed during CD and ion trap mass spectrometry measurements to avoid −SH oxidation. A stream of N_2 gas was passed over all open microfuge tubes, bottles, etc., once they were opened and again prior to closure. All CD experiments utilized aqueous solutions of AP7 (6 *μ*M), AP7C (8 *μ*M), and AP7N (12 *μ*M) at pH 7.5 in 100 *μ*M Tris-HCl buffer. All CD spectra were obtained at 20 °C with an AVIV 60 CD spectrometer, running 60DS software version 4.1t. The CD spectrometer was previously calibrated with d_{10}-camphorsulfonic acid. Wavelength scans were conducted from 185 to 260 nm with appropriate background buffer subtraction. Typical spectra were obtained as an average of three to nine scans, using 1 nm bandwidth and a scanning rate of 0.5 nm/s. Mean residue ellipticity (θ_M) is expressed in deg cm^2 $dmol^{-1}$.
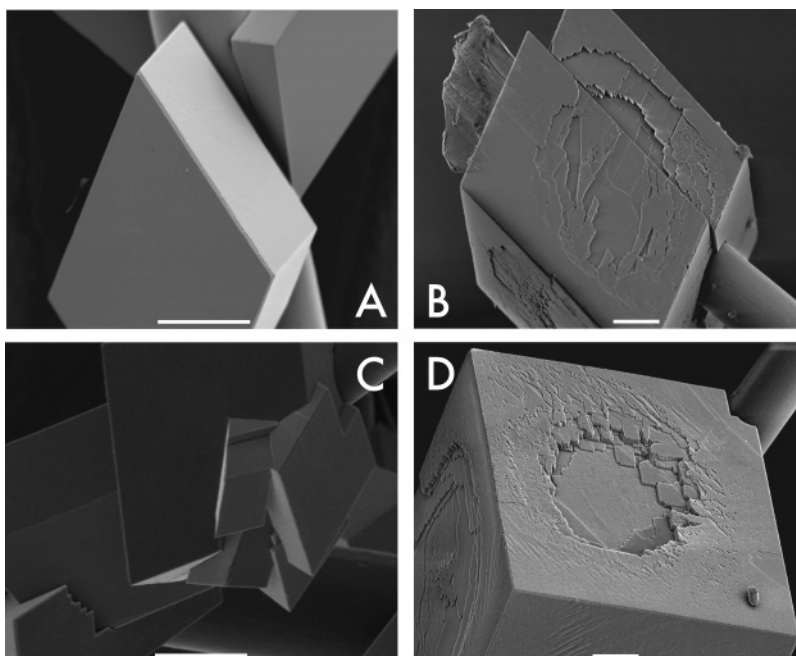
Figure 3. Scanning electron microscopy images of in vitro Kevlar calcium carbonate assay systems containing AP7 and AP7 fragments: (A) negative control assay, which features typical rhombohedral calcite crystals; (B) AP7N, 1×10^{-4} M; (C) AP7C, 1×10^{-4} M; (D) synthetic AP7 protein, 5×10^{-5} M. For all images, the scale bar is equal to 10 μm.

(c) In Vitro Kevlar Crystal Growth Assays. We employed a polyimide (Kevlar) assay for induction of calcium carbonate crystals in the presence of AP7, AP7N, and AP7C, using the modified protocol reported earlier.[21,26] For the assay, clean, HCl-treated fibers were submerged in polystyrene Petri dishes containing 3 mL of 10 mM $CaCl_2 \cdot 2H_2O$ in deionized distilled water plus the appropriate volume of polypeptide stock solutions (N_2 purged) to create final peptide assay concentrations of 1×10^{-6}, 5×10^{-6}, 1×10^{-5}, and 5×10^{-5} M for AP7 and 5×10^{-5} and 1×10^{-4} M for AP7C and AP7N. Negative control conditions consisted of no added peptide. A pinhole opening (1−2 mm) was introduced in the top of each Petri dish cover. Petri dishes were then incubated at 15 °C for 16 h in a sealed chamber (1 L volume) containing 2 g of solid $(NH_4)_2$-CO_3 (decomposition vapor method).[21,26] At the conclusion of the assay periods, Kevlar samples were washed, dried, and prepared for SEM.[21,26] SEM imaging was conducted using either an AMRAY FE-1850 cathode field emission microscope or a Hitachi S-3500N microscope at 5 kV after thin Au or Pt/Pd coating of samples. The SEM images presented in this report are representative of 20−30 different crystals in each assay sample. Cropping of SEM images and adjustment of brightness/darkness and contrast levels were performed using Adobe Photoshop.

Results and Discussion. In previous studies, AP7N exhibited concentration-dependent inhibitory activity with regard to in vitro calcium carbonate crystal growth. This subdomain gave rise to the appearance of incomplete rhombohedral calcite crystals which feature surface irregularities and blocked growth steps.[5,21] To advance our understanding of the mineral modification activity of AP7, we performed parallel characterization of the effects of synthetic AP7, AP7N, and AP7C (Figure 1) on in vitro calcium carbonate crystal growth. Using Kevlar-based assay systems (Figure 3),[20,21] we find that both synthetic AP7 and AP7N exert similar effects on the growth and morphology of rhombohedral calcite crystals (Figure 3). In particular, we note that both polypeptides promote incomplete or interrupted crystal growth and step edge rounding phenomena. Note that these effects are not observed in the negative control assay. At significantly different AP7 concentrations (5 μM versus 50 μM), the magnitude of morphological change is observed to vary, with more pronounced effects observed at higher AP7 concentrations (Figure 4). Interestingly, we note that AP7 at 50 μM appears to promote the same or slightly
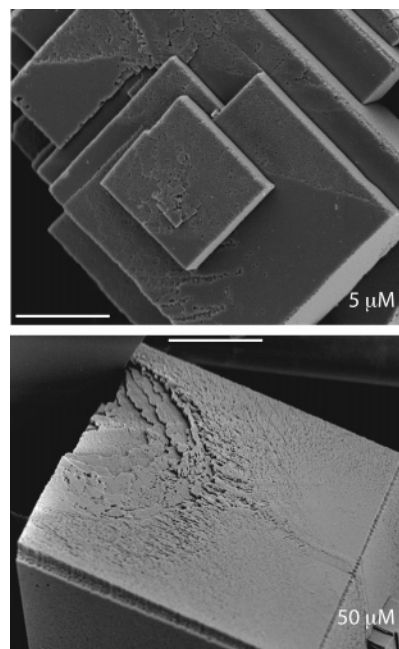

Figure 4. Scanning electron microscopy images of in vitro Kevlar calcium carbonate assay systems as a function of 5 and 50 μM AP7 concentrations. The scale bar is equal to 10 μm.

higher degree of morphological change compared to the AP7N subdomain at 100 μM (Figure 3). This suggests that the mineralization activity level of the AP7 protein may be somewhat higher than that of the AP7N subdomain itself. Interestingly, crystal growth that occurs in the presence of apo-AP7C resembles the negative control conditions (Figure 3), and we were unable to detect any significant changes in crystal morphologies or sizes in the presence of AP7C over the concentration range utilized in our study. From these observations, we conclude the following. (a) Synthetic AP7 affects calcite crystal growth in a manner consistent with previously published observations for nacre-purified AP7−AP24[5] and exhibits effects on calcite morphology that are similar to those generated
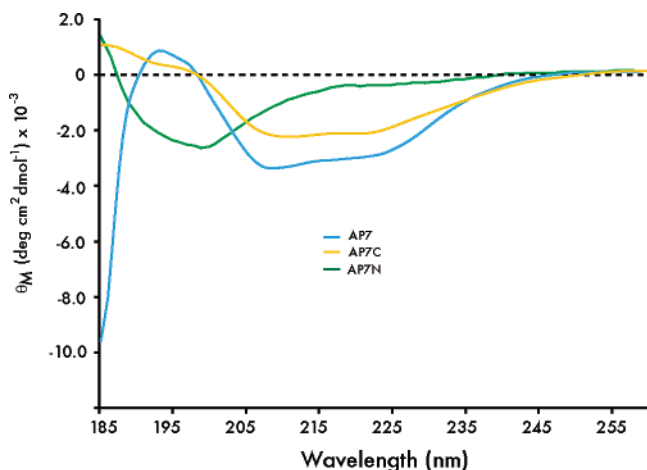
Figure 5. Far-UV CD spectra of AP7, AP7C, and AP7N polypeptide in 100 μM Tris-HCl at pH 7.5 and 20 °C.

by the N-terminal subdomain alone.[20] (b) The 30-AA N-terminal subdomain is a key player in AP7-directed mineral modification activity. (c) The C-terminal 36-AA sequence of AP7 does not directly influence calcite crystal growth under parallel in vitro conditions.

Given the results obtained from our SEM studies, we were curious to learn if each subdomain of AP7 possesses any particular structural features and how these features contribute to the overall structure of AP7. Figure 5 presents comparative CD spectra of the synthetic AP7 protein and the AP7C and AP7N model subdomains at neutral pH. As reported earlier, the far-UV circular dichroism spectrum of AP7N possesses two broad (−) absorption bands; one centered near 200 nm ($\pi-\pi*$ transition) and the other centered near 225 nm. The 200 nm $\pi-\pi*$ band is consistent with the presence of turn, extended, loop, polyproline type II, or other labile structures that exist in equilibria with random coil conformations.[5,19,20] In contrast, our present study reveals that the AP7C subdomain appears to be conformationally more stable and structured, as evidenced by the appearance of a $\pi-\pi*$ (−) band near 208 nm and an n$-\pi*$ (−) band near 222 nm, which is consistent with the presence of an α-helical secondary structure (Figure 5).[23−26] An examination of the CD spectra for AP7 at neutral pH indicates that this protein shares the same structural features of its two subdomains (Figure 5). We note the presence of a (+) band at 195 nm, indicating a random coil-like structure. Additionally, we observe the presence of (−) bands at 208 nm ($\pi-\pi*$) and 222 nm (n$-\pi*$), which are consistent with the presence of an α-helix.[23−26] Given the structural compositions of both N- and C-terminal domains (Figure 5), we conclude that each subdomain contributes different features (i.e.: AP7N, random coil; AP7C, α helix) to the observed structural organization of AP7. A more quantitative determination of AP7 secondary structure can be obtained using nuclear magnetic resonance, and these studies are currently in progress.

In summary, we have chemically synthesized and characterized a 66-AA protein associated with the aragonite polymorph formation process in mollusk nacre. This protein, AP7, exhibits concentration-dependent interruptive or inhibitory activity with calcite crystal growth in vitro and gives rise to the appearance of step edge roundening and pit formation on calcite surfaces (Figures 3 and 4). Our current data suggest that the global conformation of AP7 is a composite of the individual conformations arising from the two primary subdomains AP7N and AP7C. The fact that both AP7 and AP7C adopt a stable, helical structure in the absence of metal ions under reducing conditions supports earlier findings that the AP7 protein does not possess a true Zn(II) finger motif,[5] since the conformation of Zn(II) finger polypeptides is typically unstructured and largely random coil in conformation in the absence of

Zn(II).[22−25] Moreover, we note that two critical Zn(II) finger molecular features are absent from AP7: (a) although the 36-AA C-terminal sequence possesses −His−(X)$_6$−His, −Cys−(X)$_2$−Cys−, and −Cys−(X)$_4$−Cys− motifs, these are only partially homologous (50% match) to a known Zn(II) finger motif (i.e., the Cys$_4$ Zn(II) LIM binding domain);[5] (b) the C-terminal sequence does not possess the prerequisite Cys$_2$HisCys Zn(II) motif that is found in the LIM binding domain.[5] Hence, although AP7 possesses −His−(X)$_6$−His, −Cys−(X)$_2$−Cys−, and −Cys−(X)$_4$−Cys− motifs, it appears that these regions do not require Zn(II) or other metal ions to fold into a helical structure,[22−25] which is somewhat unusual. To gain further insight into this situation, we are currently assessing both polypeptides for metal ion interaction capabilities, and these results will be reported in a subsequent paper.

Previously, we established that the AP7N subdomain is conformationally labile[5,21,27] and exhibits concentration-dependent interruptive or inhibitory activity with calcite in vitro.[5,27] In our present study, we note that the AP7 protein generates similar results with calcite as well and, combined with the negative result obtained for the AP7C subdomain (Figure 3), it appears that the N-terminal subdomain is the primary locus of mineral modification and/or interaction activity within AP7. However, even though we were unable to detect any mineralization activity for the individual AP7C subdomain, we wish to point out that the AP7 protein, at lower concentrations, exhibits an equal or slightly higher mineralization activity level, in comparison to AP7N (Figure 3). On the basis of this observation, we cannot rule out the possibility that the overall mineral modification activity of AP7 is somehow enhanced or stabilized by the presence of the C-terminal domain. Additional studies are in progress to assess the participation of the C-terminal domain in AP7 structure and function.

Finally, we are beginning to realize that the individual protein participants in nacre layer formation are not simplistic in nature but are more complex than we initially realized and that this complexity, in part, arises from the multifunctionality[28−33] that is inherent within each individual protein sequence. On the basis of present and past studies, we believe that this may be the case with AP7, as evidenced by the following observations. (a) AP7 forms a complex with AP24.[5] (b) Recent AFM imaging studies have demonstrated that the N-terminal domain of AP7, AP7N, acts in a multifunctional capacity with regard to calcite crystal growth: it selectively blocks the growth of specific step edges while simultaneously accelerating the growth of other step edges and induces the formation of mineral deposits on calcite surfaces.[12] Similar results have been reported for other nacre-specific proteins, AP8α and AP8β.[11] (c) The overall mineral modification activity of AP7 may be enhanced by the presence of the C-terminal domain. Thus, it is likely that AP7 itself may perform more than one task within the nacre mineralization process, which, if true, would be quite interesting, given the small size of this polypeptide. Additional studies are currently in progress to determine the functional features of this protein and which regions of the AP7 sequence are responsible for specific function(s).

References

(1) Lowenstam, H. A.; Weiner, S. *On Biomineralization*; Oxford University Press: New York, 1989; pp 1−50.
(2) Levi-Kalisman, Y.; Falini, G.; Addadi, L.; Weiner, S. *J. Struct. Biol.* **2001**, *10*, 4372−4337.

(3) Weiss, I. M.; Kaufmann, S.; Mann, K.; Fritz, M. *Biochem. Biophys. Res. Commun.* **1999**, *267*, 17−21.

(4) Weiss, I. M.; Tuross, N.; Addadi, L.; Weiner, S. *J. Exptl. Zool.* **2002**, *293*, 478−491.

(5) Michenfelder, M.; Fu, G.; Lawrence, C.; Weaver, J. C.; Wustman, B. A.; Taranto, L.; Evans, J. S.; Morse, D. E. *Biopolymers* **2003**, *70*, 522−533; **2004**, *73*, 299 (errata).

(6) Thompson, J. B.; Paloczi, G. T.; Kindt, J. H.; Michenfelder, M.; Smith, B. L.; Stucky, G. D.; Morse, D. E.; Hansma, P. K. *Biophys. J.* **2000**, *79*, 3307−3312.

(7) Samata, T.; Hayashi, N.; Kono, M.; Hasegawa, K.; Horita, C.; Akera, S. *FEBS Lett.* **1999**, *462*, 225−229.

(8) Miyashita, T.; Takagi, R.; Okushima, M.; Nakano, S.; Miyamoto, H.; Nishikawa, E.; Matsushiro, A. *Marine Biotechnol.* **2000**, *2*, 409−418.

(9) Gotliv, B.-A.; Kessler, N.; Sumerel, J. L.; Morse, D. E.; Tuross, N.; Addadi, L.; Weiner, S. *ChemBioChem* **2005**, *6*, 304−314.

(10) Gotliv., B.-A.; Addadi, L.; Weiner, S. *ChemBioChem* **2004**, *4*, 522−529.

(11) Fu, G.; Qiu, R. S.; Orme, C. A.,; Morse, D. E.; De Yoreo, J. J. *Adv. Mater.* **2005**, *17*, 2678−2683.

(12) Kim, I. W.; Darragh, M.; Orme, C.; Evans, J. S. *Cryst. Growth Des*. **2006**, *6*, 5−10.

(13) Kates, S. A.; Albericio, F. In *Solid-Phase Synthesis: A Practical Guide*; Marcel Dekker: New York, 2000.

(14) Low, D. W.; Hill, M. G.; Carrasco, M. R.; Kent, S. B. H.; Bott, P. *Proc. Natl. Acad. Sci. USA* **2001**, *98*, 6554−6559.

(15) Hackeng, T. M.; Mounier, C. M.; Bon, C.; Dawson, P. E.; Griffin, J. H.; Kent, S. B. H. *Proc. Natl. Acad. Sci. USA* **1997**, *94*, 7845−7850.

(16) Miranda, L. P.; Alewood, P. F. *Proc. Natl. Acad. Sci. U.S.A.* **1999**, *96*, 1181−1186.

(17) Clayton, D.; Shapovalov, G.; Maurer, J. A.; Dougherty, D. A.; Lester, H. A.; Kochendoerfer, G. G. *Proc. Natl. Acad. Sci. USA* **2004**, *101*, 4764−4769.

(18) Bang, D.; Kent, S. B. H. *Proc. Natl. Acad. Sci. USA* **2005**, *102*, 5014−5019.

(19) Hackeng, T. M.; Griffin, J. H.; Dawson, P. E. *Proc. Natl. Acad. Sci. USA* **1999**, *96*, 10068−10073.

(20) Sydor, J. R.; Herrmann, C.; Kent, S. B. H.; Goody, R. S.; Engelhard, M. *Proc. Natl. Acad. Sci. USA* **1999**, *96*, 7865−7870.

(21) Kim, I.-W.; Morse, D. E.; Evans, J. S. *Langmuir* **2004**, *20*, 11664−11673.

(22) Clarke, N. D.; Berg, J. M. *Science* **1998**, *282*, 2018−2021.

(23) Berkovits, H. J.; Berg, J. M. *Biochemistry* **1999**, *38*, 16826−16830.

(24) Hori, Y.; Suzuki, K.; Okuno, Y.; Nagaoka, M.; Futaki, S.; Sugiura, Y. *J. Am. Chem. Soc.* **2000**, *122*, 7648−7653.

(25) Hori, Y.; Sugiura, Y. *Biochemistry* **2004**, *43*, 3068−3074.

(26) Kim, I. W.; DiMasi, E.; Evans, J. S. *Cryst. Growth Des.* **2004**, *4*, 1113−1118.

(27) Wustman, B. A.; Morse, D. E.; Evans, J. S. *Biopolymers* **2004**, *74*, 363−376.

(28) Wustman, B. A.; Weaver, J. C.; Morse, D. E.; Evans, J. S. *Langmuir* **2003**, *19*, 9373−9381.

(29) Evans, J. S. *Curr. Opin. Colloid Interface Sci.* **2003**, *8*, 48−54.

(30) Zhang, B.; Wustman, B. A.; Morse, D. E.; Evans, J. S. *Biopolymers* **2002**, *63*, 358−369.

(31) Shen, X.; Belcher, A. M.; Hansma, P. K.; Stucky, G. D.; Morse, D. E. *J. Biol. Chem.* **1997**, *272*, 32472−32481.

(32) Xu, G.; Evans, J. S. *Biopolymers* **1999**, *49*, 303−312.

(33) Zhang, B.; Xu, G.; Evans, J. S. *Biopolymers* **2000**, *54*, 464−475.